

# Diagenesis and very low grade metamorphism in a 7,012 m-deep well Hongcan 1, eastern Tibetan plateau

Hejing Wang · Yongsheng Ma · Jian Zhou ·  
Tingjing Xu

Received: 8 November 2011 / Accepted: 27 June 2012 / Published online: 9 August 2012  
© Swiss Geological Society 2012

**Abstract** This study uses clay mineral assemblages, illite “crystallinity” (IC), chlorite “crystallinity” (CC), illite polytypes, the *b* cell-dimension of K-white mica, mineral geothermo-geobarometers and homogenization temperatures of fluid inclusions to investigate the transition from diagenesis to metamorphism in a 7 km thick Triassic flysch sequence in the well Hongcan 1, eastern Tibetan plateau. The 7,012.8 m deep borehole penetrated flysch of Upper to the Middle Triassic age and represents a unique chance to characterize low temperature metamorphic processes in an unusually thick sedimentary sequence developed on thickened continental crust. Mineral assemblage analysis reveals a burial metamorphic pattern with kaolinite and chlorite/smectite mixed-layer phases present in the upper 1,500 m, and illite/smectite mixed-layer phases extending to a depth of 3,000 m. The metamorphic index mineral, graphite, was detected in sedimentary rock below 5,000 m using Raman spectroscopy. There exists a good correlation between IC and CC within the prograde burial sequence; with CC anchizonal boundaries of

0.242 and  $0.314^{\circ}2\theta$  (upper and lower boundaries, respectively) corresponding to Kübler’s IC limits at  $0.25$  and  $0.42^{\circ}2\theta$ . Illite polytypism also shows an increase in the  $2M_1$  polytype with increasing depth, with ca. 60 %  $2M_1$  abundance compared to the  $1M$  type at the surface, to 100 %  $2M_1$  at the bottom of the borehole. Fluid inclusion analysis show HHC-rich bearing fluids correspond to the diagenetic zone, CH<sub>4</sub>-rich bearing fluids appear at transitional zone from diagenetic to low anchizone and H<sub>2</sub>O-rich bearing fluids mark the high anchizone to epizone. Based on chlorite chemical geothermometer, calcite–dolomite geothermo-barometers as well as homogenization temperature of fluid inclusions, a paleotemperature range of 118–348 °C is estimated for the well with a pressure facies of low to intermediate type.

**Keywords** Diagenesis · Very-low-grade metamorphism · Illite crystallinity · Triassic flysch · Tibetan plateau

## 1 Introduction

The Triassic flysch of the Tibetan plateau preserves an important stage of tectono-thermal evolution that spans the closure of Paleo-Tethys and the formation of the Himalayas. The state of diagenesis and metamorphism of the Triassic flysch has been investigated largely by the thin section study of samples from surface outcrops (Dong et al. 1986). However, a detailed analytical study of unweathered samples from depth has not yet been undertaken. X-ray diffractometry based methods (e.g. Kübler 1964; Frey 1987) suitable for characterizing mineral assemblages in more detail have only been applied to 5 samples located far from the Hongcan 1 borehole (Xia 1993).

Since 2002 the eastern Tibetan plateau has been chosen as a new target area for oil and gas exploration, and

Editorial handling: Fernando Nieto García and Edwin Gnoss.

H. Wang (✉) · T. Xu  
Key Laboratory of Orogenic Belts and Crustal Evolution,  
Ministry of Education, Beijing, China  
e-mail: hjwang@pku.edu.cn

H. Wang · T. Xu  
School of Earth and Space Sciences, Peking University, 100871  
Beijing, China

Y. Ma  
Oilfield Exploration and Production Department, China  
Petrochemical Corporation (SINOPEC), Beijing, China

J. Zhou  
Chinese Academy of Geological Sciences, 100037 Beijing,  
China

therefore the diagenetic to low temperature metamorphic history of the Triassic flysch is of economic importance (Yang and Liu 2005). Currently, many aspects concerning the state and cause of metamorphism in the Triassic flysch are debated, with options ranging from a complete lack of metamorphism (Yang and Liu 2005) to diagenetic metamorphism (Chen et al. 2001), anchimetamorphism (Xia 1993; Wang et al. 2008), local metamorphism in the area of the Danba dome (You et al. 2006; Zhou et al. 2008), regional subgreen schist-facies metamorphism (Dong et al. 1986), regional low-temperature dynamic metamorphism (Bureau of geology and mineral resources of Sichuan province 1991) and low-grade regional dynamic metamorphism (Xu et al. 1992). Such metamorphic anomalies have been attributed to the circulation of hydrothermal fluids related to tectonic deformation, such as activity along the Longmenshan fault (cause great Sichuan earthquake on May 12, 2008) and other detachments in the Triassic flysch (Xu et al. 1992, 2007). Also unclear is the relationship between metamorphism and magmatic activity since the Mesozoic (Chung et al. 2005; She et al. 2006).

A 7,012.8 m deep well called Hongcan 1 was drilled during 2005–2006 in order to probe the depth of the Tibetan plateau as well as to explore for oil and gas in that area. The well Hongcan 1 is located within the Hongyuan County, north of Sichuan province, on the eastern margin of Tibetan plateau. Triassic flysch occurs throughout the well and represents the typical flysch sequence (200–245 Ma) of the Qingzang-Dianxi fold region located on the northern Tibetan plateau, western China (>410,000 km<sup>2</sup>, see Fig. 1). The purpose of this paper was to investigate the diagenetic to very low grade metamorphism overprint of this particularly thick Triassic flysch sequence in the well Hongcan 1 using a range of accepted geothermal indicators which have been widely used by many researchers since 1980s. Based on these new analytical results the thermal evolution of the Triassic flysch of the Tibetan plateau is addressed.

## 2 Geological setting

Tectonically the Triassic flysch in well Hongcan 1 has a complex geological history, belonging to the Songpan-Garzê orogen, which is limited by the north China, south China and Indian blocks (Xu et al. 1992, 2007; Roger et al. 2008, 2010). From Early Paleozoic to Devonian times, the Songpan area was characterized by a large carbonate platform that extended towards the SE onto the Yangtze craton. By the end of Devonian, the area underwent extensive crustal stretching with the development of ocean crust (Nie et al. 1994; Zhou and Graham 1996; Weislogel et al. 2006; Weislogel 2008). Continent–continent collision

between the North and South China blocks during the Triassic resulted in the formation of the Qinling-Dabie orogen and caused the closure of the Paleo-Tethys Ocean (Pullen et al. 2008). Large-scale foreland basins such as the Sichuan and the Songpan basins in the south developed on both sides of the collisional belt with syn-orogenic filling and closure of the basins. In the Carnian stage (T<sub>2–3</sub>), deep sea turbidites were deposited in the Songpan basin (Zhang et al. 2008). Granitoid melts intruded into the flysch series during the late Triassic to early Jurassic period (Hu et al. 2005). Early magmatism preceded deformation (Xiao et al. 2007; Weislogel 2008) or was simultaneous with folding of the Triassic strata (Hu et al. 2005). Ongoing crustal thickening and shortening finally resulted in uplift of the crust (Arne et al. 1997; Wang and Cai 2007).

Based on geophysical surveys and investigation of surface samples around Zoigê between 2002 and 2005, it was expected that the locality of the well Hongcan 1 would be in a centre of diagenetic zone and about 6 km below the surface the lower Triassic-upper Permian carbonaceous rocks would occur in which large gas reserves were found in the neighboring Sichuan basin (Ma et al. 2005, 2007). However, after drilling the borehole was discovered to be dominated by the upper-middle Triassic flysches in a sequence of alternating shales, silt- and sandstones with only minor carbonates. The current geothermal gradient of the borehole measured is 30 °C/km. The tectono-thermal evolution of the Songpan-Garzê orogen since the Mesozoic reflects the interactions between Indian and the South China and North China blocks, which was characterized by both magmatic activity and limited uplift occurred during the Mesozoic, as well as large-scale uplift and rapid cooling during the Tertiary Himalayan orogen (Huang et al. 2003).

## 3 Methods

This investigation is based on the study of 234 samples from well Hongcan 1, which including 31 core samples taken from 31 core sections. Sample preparation of clay rich rocks followed the recommendations of the IGCP 294 (Kisch 1991). Clay-sized fractions were separated using a HITACHI CR-22G centrifuge.

For XRD analyses, all measurements were performed with an X'Pert Pro MPD diffractometer with CuK $\alpha$  radiation and operating conditions of 40 kV and 40 mA. The slit system was set with a 1° divergence, an anti-scatter slit of 2° and a 6.6 mm receiving anti-scatter slit for the X'celerator detector. The step size was set at 0.017° 2 $\theta$  and the count time was 20 s. Mounts of randomly oriented bulk powder were used for mineral phase identification measured in the range of 4–75° 2 $\theta$ . Oriented slides of the

**Fig. 1** Tectonic map of China (from Ma et al. 2002). Grey area represents the Qingzang-Dianxi fold region. Filled triangle marks the location of well Hongcan 1. UHP ultrahigh pressure metamorphic belt. Lower part is the geological sketch around the well. Filled triangle marks the locality of the well Hongcan 1

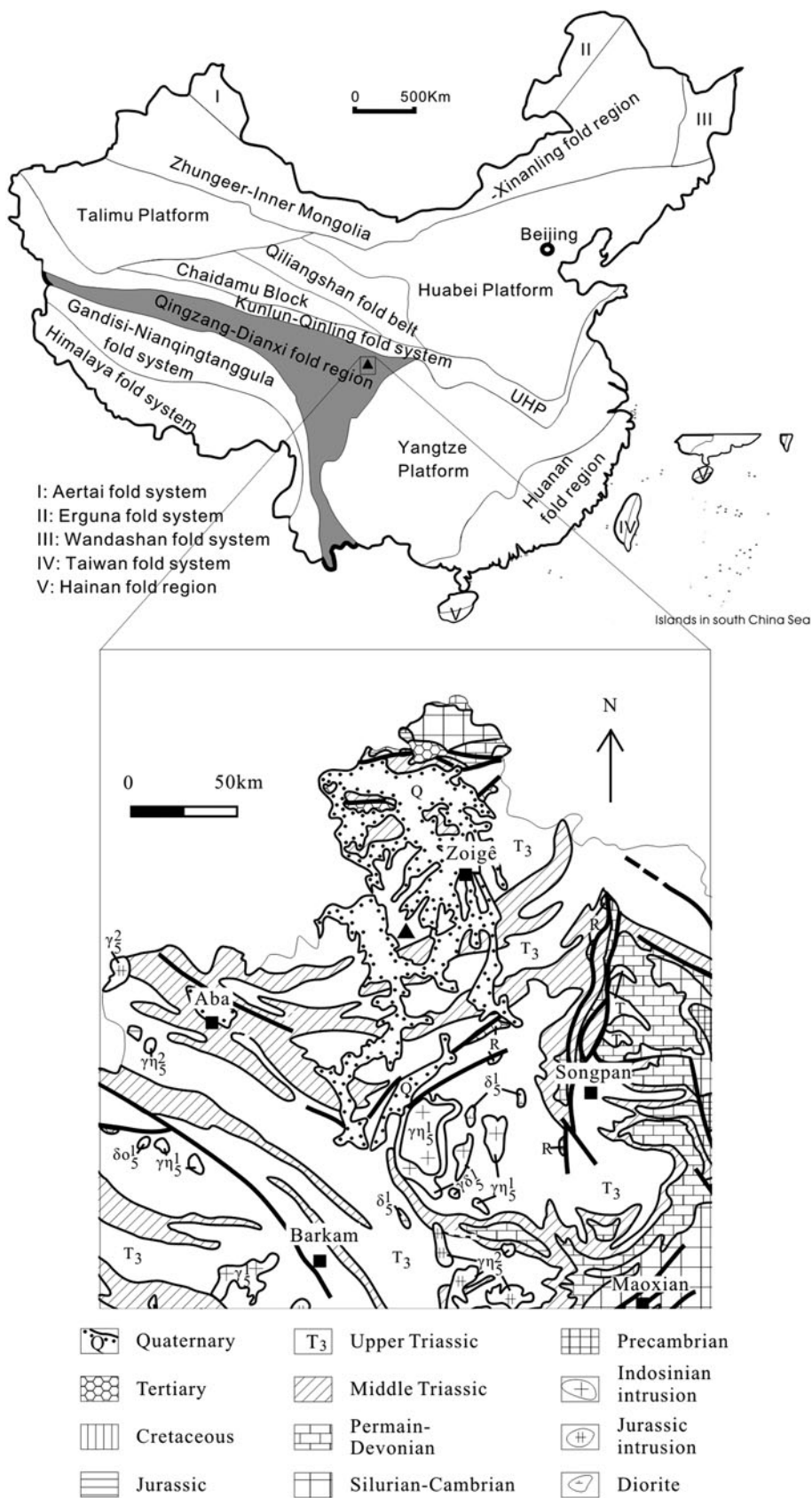


**Table 1** EMPA data of chlorite, muscovite, illite and calcite measured from rock's matrix and *b* cell data of K-white mica of part core samples and their depths

No	HW-591-3	HW-698-3	HW-699-4	HW-699-5	HW-733-2	HW-733-5	HW-733-6	HW-734-1	HW-589-2	HW-698-7	HW-699-8	HW-732-4	HW-733-4	HW-734-6	HW-589-3	HW-591-1	HW-698-1		
Depth (m)	4945.2	5847.5	6006	6543.7	6543.7	6543.7	6543.7	7011.2	4375.1	5847.5	6006	6073.2	6543.7	7011.2	4375.1	4945.2	5847.5		
Phase	Chlorite			Illite												Muscovite		Calcite	
SiO <sub>2</sub>	26.33	25.83	24.86	24.93	24.5	24.78	24.88	24.40	52.41	45.92	46.77	48.12	46.56	45.6	0.14	0.05	0.07		
TiO <sub>2</sub>	0.02	0.05	0.05	0.09	0.12	b.d.	0.08	0.10	0.43	0.35	0.19	0.30	0.44	0.24	0.04	b.d.	b.d.		
Al <sub>2</sub> O <sub>3</sub>	21.49	23.78	21.57	21.35	21.24	21.67	21.99	24.27	30.22	33.7	34.33	33.05	32.33	35.90	0.02	0.03	0.07		
Cr <sub>2</sub> O <sub>3</sub>	b.d.	0.12	0.07	0.04	0.02	b.d.	0.08	0.02	b.d.	b.d.	0.04	0.09	0.34	0.02	b.d.	b.d.	b.d.		
FeO	25.24	26.59	29.16	29.19	27.43	27.84	27.28	30.64	2.47	1.63	1.26	1.76	1.99	1.00	1.02	1.00	1.39		
NiO	0.06	0.03	0.03	0.04	0.05	b.d.	0.02	b.d.	b.d.	0.02	b.d.	b.d.	b.d.	b.d.	0.02	b.d.	b.d.		
MnO	0.05	0.07	0.06	0.04	0.03	0.13	0.05	b.d.	b.d.	b.d.	b.d.	b.d.	b.d.	0.03	1.73	0.22	0.18		
MgO	13.37	12.76	11.39	11.91	13.37	12.83	13.55	8.91	1.69	1.25	0.82	1.24	1.48	0.32	0.36	0.57	0.46		
CaO	0.27	0.08	0.13	0.15	0.11	0.04	b.d.	0.18	0.04	0.03	0.06	0.05	b.d.	b.d.	52.11	54.12	52.55		
Na <sub>2</sub> O	b.d.	0.03	b.d.	b.d.	0.03	b.d.	b.d.	b.d.	0.14	0.30	0.65	0.32	0.26	1.22	b.d.	b.d.	b.d.		
K <sub>2</sub> O	0.17	0.43	0.02	0.04	b.d.	b.d.	0.02	0.22	9.13	10.64	10.29	10.23	10.66	9.80	b.d.	0.04	0.02		
Total	86.99	89.76	87.33	87.78	86.89	87.32	87.95	88.76	96.53	93.86	94.4	95.17	94.07	94.13	55.45	56.04	54.75		
Based on	28 O			11 O												1 O			
Si	5.576	5.332	5.371	5.361	5.284	5.319	5.280	5.210	3.387	3.103	3.128	3.189	3.145	3.056	0.002	0.001	0.001		
Ti	0.003	0.008	0.008	0.015	0.019	0.013	0.013	0.016	0.021	0.018	0.010	0.015	0.022	0.012	0.001				
Al	5.364	5.785	5.492	5.411	5.398	5.482	5.500	6.107	2.302	2.684	2.706	2.582	2.574	2.836	0.000	0.001	0.001		
Cr		0.020	0.012	0.007	0.003	4.947	0.013	0.003			0.002	0.005	0.018	0.001					
Fe*	4.470	4.590	5.268	5.249	4.947	4.997	4.842	5.471	0.120	0.083	0.063	0.088	0.101	0.050	0.014	0.014	0.020		
Ni	0.010	0.005	0.005	0.007	0.009		0.003			0.001					0.000				
Mn	0.009	0.012	0.011	0.007	0.005	0.024	0.009							0.002	0.025	0.003	0.003		
Mg	4.221	3.926	3.668	3.818	4.298	4.105	4.287	2.836	0.163	0.126	0.082	0.123	0.149	0.032	0.009	0.014	0.012		
Ca	0.061	0.018	0.030	0.035	0.025	0.009		0.041	0.003	0.002	0.004	0.004			0.948	0.966	0.963		
Na		0.012			0.013				0.018	0.039	0.084	0.041	0.034	0.159					
K	0.046	0.113	0.006	0.011		0.005	0.005	0.060	0.753	0.917	0.878	0.865	0.919	0.838		0.001	0.000		
T(°C)			213 <sup>†</sup>	237 <sup>†</sup>	348 <sup>†</sup>	328 <sup>†</sup>	317 <sup>†</sup>												
X <sub>Mg</sub>	0.486	0.461	0.410	0.421	0.465	0.451	0.470	0.341											
Al <sup>IV</sup>	2.424	2.668	2.629	2.639	2.716	2.681	2.720	2.790	0.613	0.897	0.872	0.811	0.855	0.944					
Al <sup>VI</sup>	2.94	3.117	2.863	2.772	2.682	2.801	2.78	3.317	1.689	1.787	1.834	1.771	1.718	1.892					
ΣOcta	11.631	11.633	11.799	11.839	11.927	11.903	11.909	11.624	1.972	1.996	1.979	1.982	1.968	1.974					
K+Na									0.770	0.956	0.962	0.906	0.953	0.996		0.001	0.000		
R1									0.283	0.209	0.145	0.210	0.250	0.082					
R2									0.934	0.956	0.967	0.953	0.944	0.974					
															264	316	293		
															0.938 <sup>§</sup>	1.424 <sup>§</sup>	1.179 <sup>§</sup>		

Table 1 continued

No	HW-591-3	HW-698-3	HW-699-4	HW-699-5	HW-733-2	HW-733-5	HW-733-6	HW-734-1	HW-589-2	HW-698-7	HW-699-8	HW-732-4	HW-733-4	HW-734-6	HW-589-3	HW-591-1	HW-698-1
a1 <sup>¶</sup>		0.00036783	0.00046595	0.00092126	0.00070864	0.00090551											
a2 <sup>¶</sup>		0.00244637	0.00271166	0.00431985	0.00381852	0.00460479											
a3 <sup>¶</sup>		0.05127978	0.04885852	0.03564009	0.03889698	0.03319854											
a4 <sup>¶</sup>		0.00762870	0.00607520	0.00310834	0.00349319	0.00420941											

$\Sigma Octa$  octahedral occupancy,  $Rl = Mn+Mg+Fe$ ,  $R2 = \frac{VI}{Al^{VI}}(\frac{VI}{Al^{VI}} + \frac{VI}{Fe^{VI}})$ , *b.d.* Bleow. detection limit

\* For muscovite and illite the FeO is treated as  $Fe_2O_3$

§  $X_{Mg}^{Cc}$

¶ Calculated by Inoue et al. (2009) method, those parameters  $a1$ ,  $a2$ ,  $a3$  and  $a4$  for temperature calculation are given in the eighth decimal and their meanings refer to Inoue et al. (2009)

$<2 \mu m$  fraction were measured from 4 to  $35^\circ 2\theta$  for clay mineral identification and IC and CC measurements. Because nearly all samples contain quartz, this mineral was used as an internal standard to make peak shift corrections.

For chemical composition analysis of minerals, electron microprobe analyses (EMPA) were performed using a JXA-8100 electron microprobe at 15 kV acceleration voltage and 10 nA beam current, a  $1 \mu m$  beam diameter, a PRZ correction, and calibration against 53 minerals standards of SPI Corp. Ltd, USA. All Fe was calculated as FeO. The thin sections for EMPA were oriented perpendicular to the rock fabric in order to reduce the influence of neighboring mineral grains.

Fluid inclusion analysis was performed with a MXM850 heating-cooling stage installed on an Olympus microscope system. The temperature was adjustable from room temperature up to  $400^\circ C$  with a temperature resolution of  $0.1^\circ C$ . The objective lens used was 32X. Thin sections were prepared from those flysch samples containing a quartz veins lying parallel or subparallel to the bedding fabric.

Raman spectra were obtained with a confocal micro Raman system Reshan-1000 and an excitation wavelength for 514.5 nm line for an Ar ion laser operated at 50 mW. The scanning range was  $3,000\text{--}500 \text{ cm}^{-1}$  with 10 s counting time. Each spectrum was measured with a  $20\times$  objective and in single accumulation mode. The resolution was  $\pm 1 \text{ cm}^{-1}$ . Inorganic carbonaceous materials were collected from black flysch samples after treatment with HF and HCl acids.

IC was measured as the full width at half maximum (FWHM) of the ca. 1 nm XRD reflection (002) of the white mica (illite) phase. The width expressed in  $^\circ \Delta 2\theta$  using  $CuK\alpha$  radiation is known as the Kübler Index (Kübler 1964) and was calibrated based on a set of IC standards provided by Warr and Rice (1994). The IC boundaries for the anchizone are 0.25 and  $0.42^\circ \Delta 2\theta$  and equivalent CC measurements were made using the FWHM of the chlorite (002) reflection (Árkai and Ghabrial 1997). Mixed-layer illite/smectite (I/S) phases were detected on the bases of the variations of the 1 nm “complex” reflection after glycolation, and heat treatment at  $375^\circ C$  for an hour.

Determination of illite polytypes were performed by XRD method using random preparations measured over the diffraction range of  $25\text{--}32^\circ 2\theta$ , where the diagnostic reflections for  $2M_1$  and  $1M$  polytype of illite could be identified. Decomposition procedures were used to separate the interference peaks overlapping the (112) reflection of  $1M$  structure and the (025) reflection of the  $2M_1$  structure of illite whereby all fitting reliabilities were below 3 %.

The *b* cell dimension of K-white micas was calculated from the relation  $b = d_{(060, -331)} \times 6$  in which the  $d_{(060, -331)}$  was measured using the quartz reflection (211) as an internal standard.

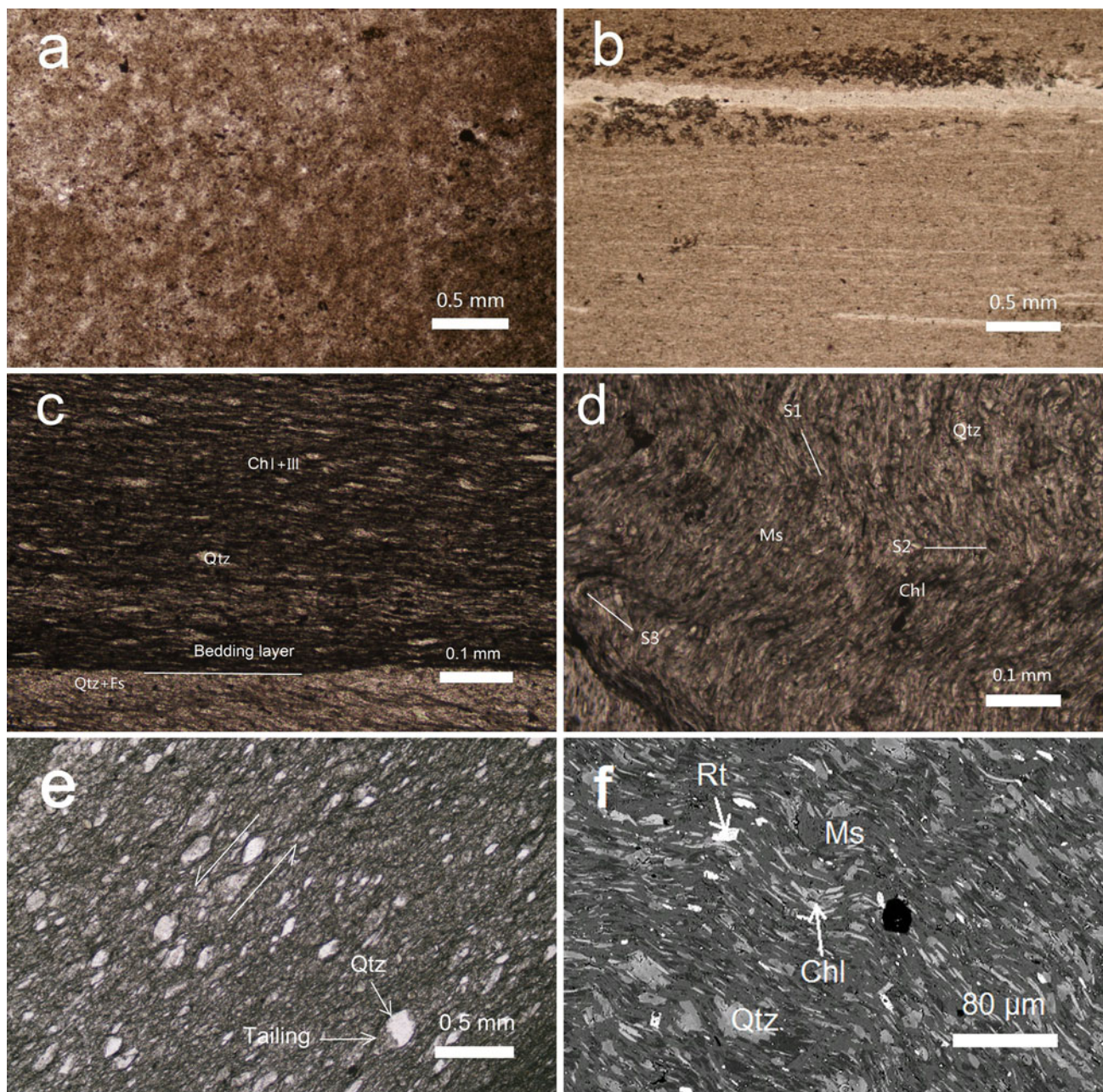


**Fig. 2** Texture variation with depth. **a** Mudrock, single polar, 100 m, HW-511, no orientation was observed in clay matrix. **b** Shale, single polar, 358.4 m, HW-446, sedimentary lamination keeps well. **c** Slate, single polar, 4375.1 m, HW-589, new formed clay minerals grow approximately along bedding layer. **d** Phyllite, single polar, 7011.2 m, HW-734, phyllitic structure, penetrative schistosity with

three deformation phases developed. **e** Mylonite, single polar, 6073.2 m, HW-732, augen structure. **f** Back-scattered electron scanning microscopy image, microtexture of phyllite, 7011.2 m, HW-734, matrix is dominated by chlorite and muscovite; micro crenulation can be observed. *Qtz* quartz, *Fs* feldspar, *Ms* muscovite, *Chl* chlorite, *Ill* illite, *Rt* rutile

For chlorite chemical geothermometry (Inoue et al. 2009), EMPA data from core samples collected from the high anchizone and anchi-epizone transition were used. Such HA and A-E rocks are assumed to have attained equilibrium and thus be suitable for mineral geothermometer application. For calcite geobarothermometry, the pressure condition is referred to about 3 kbar. See Sect. 4.6 for detail.

**4 Results and discussions**

**4.1 Mineral assemblages**

The main mineral phases recorded throughout borehole are quartz, feldspar, illite or muscovite and chlorite. Diagenetic minerals, namely mixed-layer illite/smectite (*I/S*) and chlorite/smectite (*C/S*) phases, and kaolinite occur between

0–3,042, 0–40 and 1,000 m respectively. The ordering type of I/S is  $R \geq 1$  and the amount of smectite in I/S ranges from 12 to 23 %. C/S is a randomly ordering type. The metamorphic index mineral graphite was found in several segments below 5,038 m depth. EMPA composition data for calcite, illite, muscovite and chlorite is listed in Table 1.

#### 4.2 Rock fabric

Figure 2 shows the changes in rock fabric with depth, which range from mudrocks and shales at the surface to slates, phyllites and even mylonites toward the bottom of the borehole. The various textural zones contain rocks with clay matrixes change from illite–smectite and chlorite–smectite assemblages to more crystalline muscovite–chlorite assemblages at depth. Mudrocks (Fig. 2a, 100 m) are characterized by no preferred orientation in the matrix, whereas the shales (Fig. 2b, 358.4 m) contain a sedimentary fabric within the clay matrix forming a thin beds and lamination. Illite–chlorite bearing slates (Fig. 2c HW-589, 4,375.1 m) are characterized by new formed phyllosilicates orientating at low-angles to the sedimentary bedding. Muscovite–chlorite phyllites (Fig. 2d, 7,011.2 m) contain neocrystallized phyllosilicates forming a series of cleavages penetrating the rocks, with strain-induced segregation of quartz and feldspar forming syn-tectonic mineralization. Three deformation cleavages S1–S3 were observed. S1 is penetrative and comprises of chlorite and muscovite (previously referred to as sericite, Rieder et al. 1998). This cleavage was overprinted by the S2 cleavage at an angle of  $68^\circ$ . S3 is restricted to a localized area and has an angle of  $40^\circ$  to S2. Because it is not possible to locate all three fabrics in the cored rocks, the observed S1–3 deformation phases cannot be directly linked to other geological structures. Mylonites contain (Fig. 2e, 6,073.2 m) an elongated and mortar texture of corroded quartz porphyroclasts and feldspar that occasional contain pressure shadows filled with newly formed phyllosilicates. While most quartz porphyroclasts are elongated and rounded into to form augen like structures, some asymmetrical clasts indicate a sinistral shear sense (shearing direction is marked by a pair of arrows in Fig. 2e).

#### 4.3 Illite “crystallinity” and chlorite “crystallinity”

IC values from well Hongcan 1 range between 0.234– $0.679^\circ\Delta 2\theta$  and CC values between 0.214– $0.477^\circ\Delta 2\theta$ . From the top to the bottom of the borehole, the IC Kübler index generally decreases from  $>0.60$  to ca.  $0.25^\circ\Delta 2\theta$  (Fig. 3). Adopting accepted anchizone boundaries at 0.42 for the lower limit and  $0.25^\circ\Delta 2\theta$  for the upper limit (Kübler 1964; Merriman and Peacor 1999), the well can be

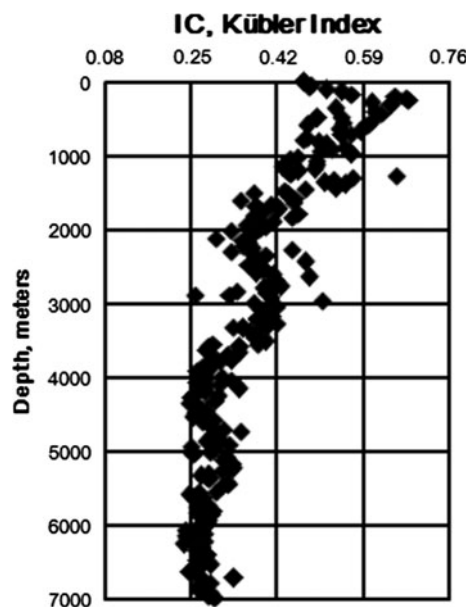


Fig. 3 Variation of IC with depth in well Hongcan 1

divided into the diagenetic zone (D, above 1,500 m), a transition from diagenetic zone to anchizone (D-LA, 1,500–3,270 m), the low anchizone (LA, 3,270–5,470 m), the high anchizone (HA, 5,470–6,000) and a transitional section from high-anchizone to epizone (HA-E,  $>6,000$  m). A good correlation (Fig. 4) between IC and CC was derived as:

$$IC = 2.9714CC^{1.7101} \quad (R^2 = 0.857, N = 233). \quad (1)$$

Based on this correlation the boundaries of anchizone in terms of CC values are  $0.314$  and  $0.242^\circ\Delta 2\theta$  for the lower and upper limits. If weathered near surface sample (HW-462) is excluded as well as sandstone and meta-sandstone lithologies, an even better correlation between IC and CC within those core samples is obtained as  $IC = 5.356CC^{2.17}$ , ( $R^2 = 0.912, N = 27$ ). Weathering has likely oxidized the  $Fe^{+2}$  in chlorite to  $Fe^{+3}$  causing changes in the chlorite structure and alterations to crystallinity. The lack of correlation for many surface samples was also noted by Wang et al. (1996). Due the narrow range of CC values across the anchizone (only  $0.07^\circ\Delta 2\theta$ ) this zone was not further subdivided when based on CC measurement.

#### 4.4 Illite polytypes

As pointed out by Frey (1987), the illite polytype transformation from  $1M_d$  to  $2M_1$  can be used as an indicator of the state of diagenesis and very low grade metamorphism. The illite polytype in well Hongcan 1 was investigated by XRD analyses of random powder preparations which uses the integrated intensity ratio  $P = 2M_1(I_{025})/[1M(I_{112}) + 2M_1(I_{025})]$ , see Fig. 5 for detail. The total range of P in the

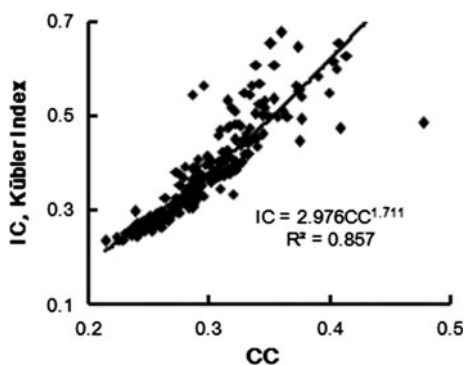


Fig. 4 Correlation between IC and CC

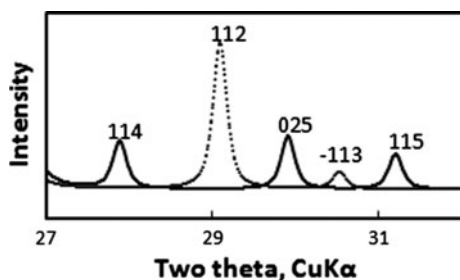


Fig. 5 Measurement of illite polytype parameter  $P = 2M_1(I_{025}) / [1M(I_{112}) + 2M_1(I_{025})]$ . There is a major difference between  $1M$  and  $2M_1$  structures of illite, that is,  $d_{112}$  (3.66 Å) of  $1M$  illite and  $d_{025}$  (2.988 Å) of  $2M_1$  illite (according to ICDD 2005). Because  $d_{114}$  of  $2M_1$  structure is often interfered by feldspar's major reflections specially by the main reflection (3.19 Å) of albite and  $d_{-113}$  is too weak, the amount of  $2M_1$  in the mixture of  $1M + 2M_1$  is measured and calculated using the integrated intensities of reflection (112) of  $1M$  and (025) of  $2M_1$  illite for the sake of simplification. When other reflection appears the deconvolution technique was used and this way the pure reflections of 025 and 112 can be obtained

well is 0.4–1 and from the surface to the bottom, a general increasing tendency of  $P$  exists from ca. 0.6–1. However, because of the presentation of detrital mica the  $P$  is enhanced and 0 values for  $P$  in diagenetic rocks is not to be expected. Below 3,000 m the  $P$  increases, on average, to 0.61 at 3,000 m, to 0.73 between 3,000–4,000 m, to 0.94 between 4,000–5,000 m, to 0.98 between 5,000–6,000 m and to 0.99 at depths >6,000 m. A poor power functional correlation between IC and  $P$  is derived as:

$$IC = 0.270P^{-0.97} \quad (N = 232, R^2 = 0.718) \quad (2)$$

#### 4.5 Quartz fluid inclusions

Some quartz veins were collected from core samples which occur parallel and subparallel to bedding ( $S_0$ ). The homogenization temperature and composition of fluid inclusions were determined and assuming constant composition and volume since trapping (Mullis 1987; Mullis et al. 2002), the results could be used to determine the lower limit of formation temperatures. Three populations of homogenization temperatures (Table 2) could be recognized that could also be distinguished by features of quartz morphology (Mullis 1987). The diagenetic zone contained primary quartz inclusions with the lower homogenization temperatures and compositions relatively rich in HHC. The quartz fluid inclusions found in high anchizone show a broad temperature range typical for both diagenetic to metamorphism conditions but are notably rich in  $H_2O$ . This mixture of homogenization temperature within the quartz particle is considered to represent its long growth history. In these samples, the  $CH_4$  and the  $H_2O$  Raman shifts were successfully detected at 2,914 and 3,000–3,300  $cm^{-1}$  corresponding to LA and A-E zones respectively (see Fig. 6).

Table 2 Geo-thermometric data from part core samples

No.	Depth (m)	$T_{(Cc-Do)}^a$ (°C) <sup>d</sup>	$T_{(Ch)}^b$ (°C) <sup>d</sup>	$T_h^c$ (°C)
HW-462	0			184, 189, 188
HW-447	469.4			129, 118, 135, 138, 169, 179, 181, 157
HW-458	1949			154, 185
HW-589	4375.1	264		
HW-591	4945.2	316		
HW-698	5847.5	293		
HW-699	6006		213, 237	
HW-732	6073.2			179, 159, 170, 150, 287, 163, 236, 235, 218, 239
HW-733	6543.7		328, 348, 317	133, 139, 152, 157, 177, 174, 174, 235, 270, 273, 230, 249, 156, 176, 161, 192, 166
HW-734	7011.2			232, 223, 235

<sup>a</sup> Temperature evaluated from calcite geobarometer, 3 kbar pressure condition has been considered according to  $b$  cell geo-barometry of K-white mica and the erosion and depth of Triassic in the well, see text for detail

<sup>b</sup> Temperature evaluated from chlorite chemical geothermometer (Inoue et al. 2009)

<sup>c</sup> Homogenization temperature of fluid inclusion in quartz

<sup>d</sup> Calculated from EMPA data

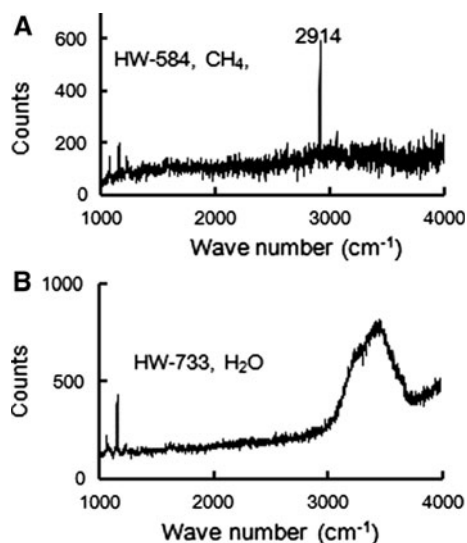


**Fig. 6** Raman spectroscopy of fluid inclusion trapped in quartz. **a** Methane and **b** water

#### 4.6 Metamorphic pressure evaluation

Statistical analyses and cumulative frequency patterns of the K-white mica *b* cell parameter has been well investigated in metamorphic terrains of different types ranging from low to high pressure facies (Sassi and Scolari 1974). Metamorphic pressure plays a role in affecting the composition of mica series, with substitutions in IV and VI sites, as well as in the interlayer (Guidotti and Sassi 2002). Structural analysis (based on ionic radii calculations, Shannon 1976) indicates that the substitutions with increasing pressure of  $\text{Fe}^{2+}\text{Mg} \leftrightarrow \text{Al}^{3+}$  and  $\text{Fe}^{3+} \leftrightarrow \text{Al}^{3+}$  within octahedrons plays a more important role in impacting mica structure than the  $\text{Si}^{4+} \leftrightarrow \text{Al}^{3+}$  substitution in tetrahedrons. This is in agreement with the statistic results of K-white mica geobarometer. From this point of view, it is reasonable and reliable to use the K-white mica *b* cell geobarometer in the study of metamorphic pressure evaluation for very low grade metamorphism of clastic rocks.

Table 3 lists these describing substitutions in muscovite and chlorite and the exchange coefficient  $K_D$  of the Tschermak substitution between muscovite and chlorite. The meanings of the ratio of *t*, *p* and  $K_D$  are referred to Miyashiro and Shido (1985). It shows from Table 3 that *t*, *p* and  $K_D$  increase to a top (5,847–6,073 m) and then decrease consistently. This indicates that the amount of celadonite in muscovite and antigorite in chlorite increase and then decrease (Miyashiro and Shido 1985).

Being a species of the mica group, the illite *b* cell dimension has the same meaning as the muscovite *b* cell and has been widely used as a mica *b* cell geobarometer by many researchers (Padan et al. 1982; Yang and Hesse

**Table 3** *t*, *b* cell and  $\text{Na}/(\text{Na} + \text{K})$  of muscovite, *p* of chlorite and  $K_D$  of Tschermak substitution between muscovite and chlorite from core samples in HA and A-E

No.	Depth (m)	<i>b</i> cell (nm)	$\text{Na}/(\text{Na} + \text{K})$	<i>t</i>	$K_D$	<i>p</i>
HW-698	5847.5	0.9011	0.041	0.103	0.23	0.333
HW-699	6006	0.9005	0.087	0.128	0.281	0.343
HW-732	6073.2	0.9013	0.045	0.189	0.414	0.36
HW-733	6543.7	0.9013	0.036	0.145	0.345	0.33
HW-734	7011.2	0.8995	0.159	0.056	0.137	0.303

$t = \text{Si} - 3$  (formula of muscovite is calculated based on 11 oxygen);  $p = (\text{Si}/2 - 2)/2$  (formula of chlorite is calculated based on 28 oxygen);  $K_D = [t/(1 - t)]/[p/(1 - p)]$ ; see Miyashiro and Shido (1985)

1991; Wang et al. 1996; Gutierrez Alonso and Nieto 1996; Cruz and Jiménez 2002; Bozkaya and Yalçın 2005; Potel 2007; Brime et al. 2008; Kemp and Merriman 2009; Corrado et al. 2010; Offler et al. 2011). K-white mica *b* cell values of 52 samples were measured from the Triassic flysches in well Hongcan 1. The values range from 0.8992 to 0.9023 nm, with an average of 0.9008 nm. As derived from the cumulative frequency curves of the *b* cell values (Fig. 7), the pressure condition below 5,470 m (HA to A-E) is a little lower than the N. New Hampshire pressure type (low intermediate, Rumble 1973; Guidotti and Sassi 1986). According to Guidotti and Sassi (1986) the average *b* cell value of core samples (9.008 Å, close to the 9.010 Å line) corresponds to c. 3 kbar, for the high anchizone (HA)

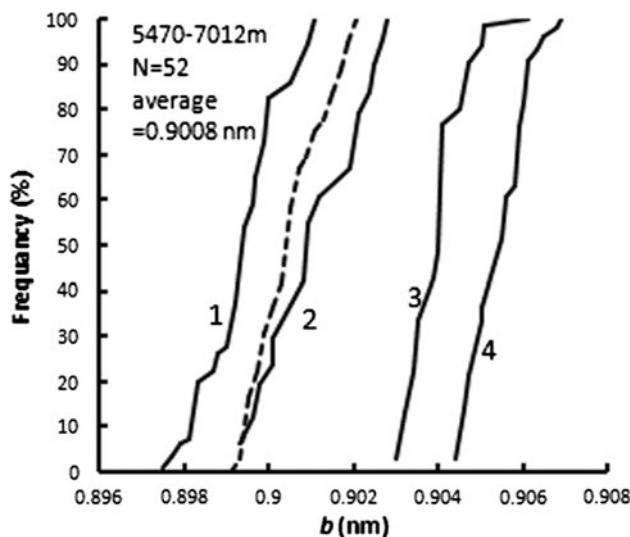


**Fig. 7** Cumulative frequency curves of K-white mica *b* cell dimension. *Solid line 1* Bosos low pressure type, *solid line 2* N. New Hampshire low intermediate pressure type, *solid line 3* Otago intermediate high pressure type, *solid line 4* Sanbagawa high pressure type, *shaded line* represents the cumulative frequency curves of K-white mica *b* cell dimensions from HA and A-E transition (5,470–7,000 m)

and anchi-epizonal (A-E) equivalent temperatures. The estimated erosion (>3.8 km) and depth (7 km) of Triassic in the well Hongcan-1 (Bureau of geology and mineral resources of Sichuan province 1991; Li et al. 2006) are also compatible with pressure condition around 3 kbar.

#### 4.7 Temperature evaluation

The chlorite chemical geothermometer (Inoue et al. 2009), calcite–dolomite (Cc–Do) geobarometer (Goldsmith et al. 1955; Goldsmith and Newton 1969; Bickle and Powell 1977; Turner 1981) and homogenization temperature of quartz fluid inclusions were used to evaluate the metamorphic peak temperature of Triassic flysches in well Hongcan 1. All temperature data are listed in Table 2. Because application of mineral geothermometer requires equilibrium assemblages only flysch of the HA and A-E transition was used (Note in Fig. 3f the chlorite and muscovite in the A-E transition sample are in equilibrium). Chlorite is composed by two tetrahedral and two octahedral sheets, the temperature would impact on both of them. It is clear that chlorite Al IV site geothermometer (Cathelineau 1988) obtains temperature information only from empirical data about IV site while the chlorite chemical geothermometer (Inoue et al. 2009) calculates temperature, using a thermodynamic approach from both IV and VI sites. For this reason we have chosen the chlorite chemical geothermometer for temperature evaluation.

X-ray diffractometry is a more statistically valid approach as it measures countless small particles of minerals without limitations in dimension and it has been widely used in analyzing very low grade metamorphic rocks. It is well known that rocks of greenschist facies and higher metamorphic facies are well crystallized and when their minerals are in equilibrium those geothermometers and geobarometers can be applied. However, it should keep in mind that minerals in equilibrium should not be limited by the effective resolution of the microscope (2  $\mu\text{m}$ ) or EMPA (1  $\mu\text{m}$ ). Minerals in equilibrium can rationally be less than 1–2  $\mu\text{m}$  in size. The general temperatures variations with depth in the well Hongcan 1 based on all methods are shown in Fig. 8. All indicate increasing temperatures with decreasing depth in the Triassic flysch corresponding to the diagenetic to epizonal transition.

The tectono-thermal history can be summarized as follows. Following deposition in a deep sea environment of the Paleo-Tethys ocean, and accumulations of roughly 5–7.5 km thick turbidites in the Songpan basin during the Carnian stage ( $T_{2-3}$ ) (p219, the Bureau of Geology and Mineral Resources of Sichuan Province 1991), collision between the south and the north China blocks caused a folding of Triassic flysches (see the geological sketch around the well in Fig. 1) and structural thickening of the

sequence to over 7 km in the well Hongcan 1 or 10–15 km in the area near Zoigê (closed fold or intrafolial fold produced in the Triassic flysch strata an increase of, at least, 2 times in thickness, Zhao et al. 2004). Structural overloading in a foreland basin setting is suggested to have been responsible for the increasing temperature at depth (350 °C/10 km for a normal gradient 35 °C/km), inducing anchimetamorphism at the bottom of Triassic flysches. This temperature agrees well with 348 °C evaluated from the chlorite chemical geothermometer. With increasing depth, the decreasing of IC and CC, increasing of P, rock fabric evolution from no preferred orientation in the matrix to penetrating cleavages, fluid inclusion in quartz from HHC zone to  $\text{CH}_4$  and to  $\text{H}_2\text{O}$  zone and the mineral assemblage from illite-I/S–C/S–chlorite to muscovite–chlorite; all of them consistently indicate the increase in grade. “Fold overloading model” is therefore proposed to describe the anchimetamorphism of the Triassic flysches in the well. In the eastern Sichuan basin, the neighboring area, where the Triassic consists of about 1,800 m carbonaceous limestone of  $T_{1-2}$  and 1,500 m clastic rocks of  $T_3$ , the structural overloading was not able to cause very low grade metamorphism due to the thinner thickness of the Triassic strata. Post-metamorphic structural movements (shearing) produced a series of detachments within the Triassic flysches (mylonites) at different levels of the well, which were related to the development of S2–3 cleavages. The Xianshuihe fault produced a strike-slip movement in the early Tertiary and disturbed the distribution of metamorphic zones (Wang et al. 2011). Finally the Himalayas movement caused uplift and denudation of the Triassic flysch (>3.8 km erosion since Cretaceous, Bureau of geology and mineral resources of Sichuan province 1991, Li et al. 2006), but this final event had little influence on the distribution of the very-low grade metamorphic rocks.

## 5 Conclusions

The 7 km thick Triassic flysch sequence penetrated by well Hongcan 1 shows a continuous increase in metamorphic grade with depth ranging from late diagenesis in the upper 1,500 m to epizonal conditions at bottom of the borehole.

Fluid inclusions within quartz from core samples are consistent with the grade changes with a higher hydrocarbon zone corresponding to the diagenetic rocks, a methane zone within the diagenetic to anchizone rocks and a water zone ( $\text{H}_2\text{O}$ ) corresponding to the anchizone–epizone transition.

The peak metamorphic pressure condition experienced by the Triassic flysch was slightly lower than the intermediate–low pressure conditions and peak temperature reached 348 °C. The diagenetic to epizonal metamorphism

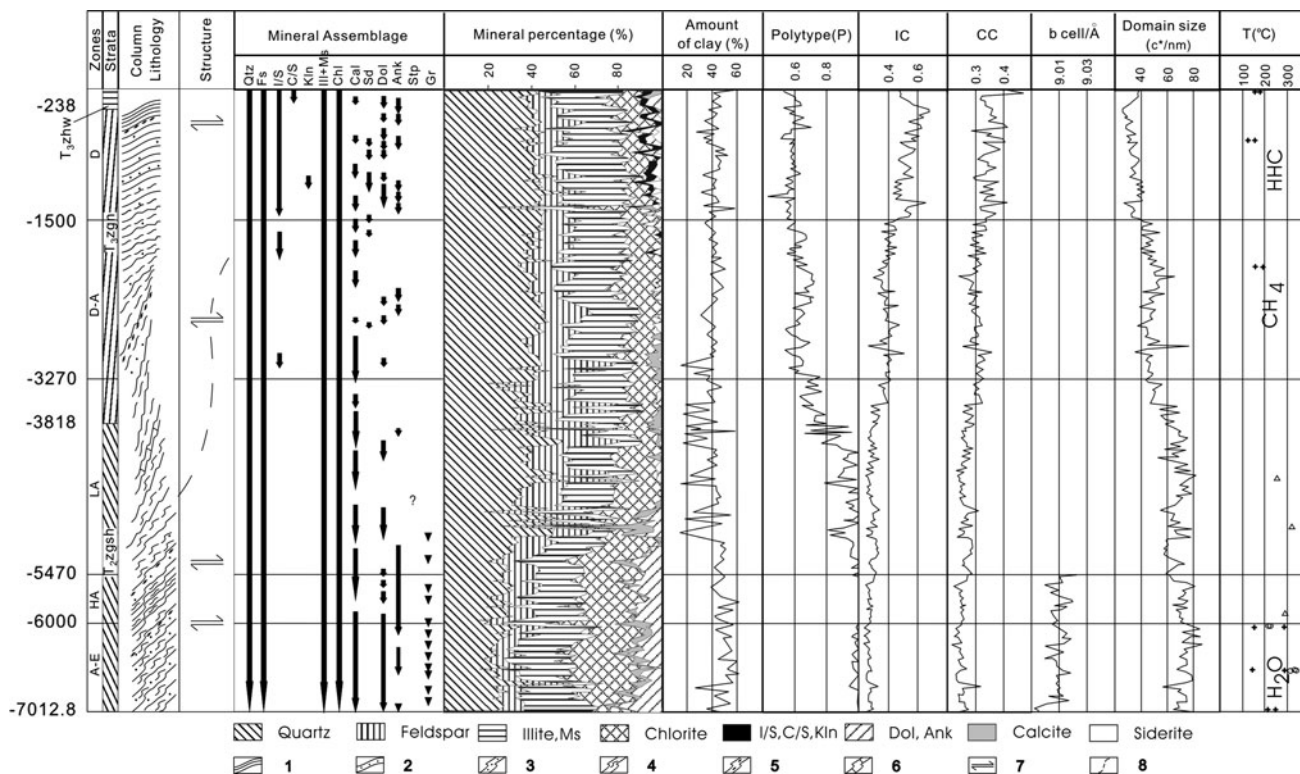


**Fig. 8** Comprehensive variations of all evolutionary parameters from diagenesis to very low grade metamorphism with depth of well Hongcan 1. *D* diagenetic zone, *D-A* transition between diagenetic zone and anchizone, *LA* low anchizone, *HA* high anchizone, *A-E* transition between anchizone and epizone, *T<sub>3zhw</sub>* Zhuwu formation of upper Triassic, *T<sub>3zgn</sub>* Zagunao formation of upper Triassic, *T<sub>2zgh</sub>* Zagashan formation of middle Triassic, *Qtz* quartz, *Fs* feldspar, *Ill* illite, *Ms* muscovite, *Chl* chlorite, *I/S* illite/smectite mixed-layer phase, *C/S* chlorite/smectite mixed-layer phase, *Kln* kaolinite, *Cal* calcite, *Sd* siderite, *Dol* dolomite, *Ank* ankerite, *Sp* stilpnomelane, *Gr*

graphite, *IC* “illite crystallinity”, *CC* “chlorite crystallinity”,  $P = 2M_{025}/(2M_{025} + 1M_{112})$ , *HHC* higher hydrocarbons, *CH<sub>4</sub>* methane, *H<sub>2</sub>O* water, *T* formation temperature. Numbers with a minus sign by the left of column indicate the depth down from the ground surface. *Legend 1* shale, 2 fine sandstone, 3 meta-sandstone, 4 slate, 5 phyllite, 6 marble, 7 detachment, 8 folding trace. *Plus sign* indicates homogenization temperature of fluid inclusion in quartz; *triangle* indicates temperature evaluated by Cc–Do geobarothermometry; *open circle* indicates temperature evaluated by chlorite chemical geothermometer (Inoue et al. 2009)

of the studied sequence reflects structural thickening of the Triassic sedimentary rocks.

**Acknowledgments** The first author had been grateful to Prof. Martin Frey who guided him to the field of very low grade metamorphism during 1990–2000. We also thank Prof. F. Nieto’s effort on this paper and two anonymous reviewers’ comments. This study is supported by the project of SINOPEC Group No. G0800-05-ZS-(KJ-05-06) and the National Natural Science Foundation of China (Grants No. 40972038, 40872034 and 40572032).

**References**

Árkai, P., & Ghabrial, D. S. (1997). Chlorite crystallinity as an indicator of metamorphic grade of low-temperature meta-igneous rocks: A case study from the Bukk mountains, northeast Hungary. *Clay Minerals*, 32, 205–222.  
 Arne, D., Worley, B., Wilson, C., Chen, S. F., Foster, D., Luo, Z. L., et al. (1997). Differential exhumation in response to episodic thrusting along the eastern margin of the Tibetan plateau. *Tectonophysics*, 280, 239–256.

Bickle, M. J., & Powell, R. (1977). Calcite–dolomite geothermometry for iron-bearing carbonates. *Contributions to Mineralogy and Petrology*, 59, 281–292.  
 Bozkaya, Ö., & Yalçın, H. (2005). Diagenesis and very low-grade metamorphism of the Antalya unit: Mineralogical evidence of Triassic rifting, Alanya-Gazipaşa, central Taurus belt, Turkey. *Journal of Asian Earth Sciences*, 25, 109–119.  
 Brime, C., Perri, M. C., Pondrelli, M., Spalletta, C., & Venturini, C. (2008). Polyphase metamorphism in the eastern Carnic Alps (N Italy-S Austria): Clay minerals and conodont Colour Alteration Index evidence. *International Journal of Earth Sciences*, 97, 1213–1229.  
 Bureau of geology and mineral resources of Sichuan province (1991). *Regional geology of Sichuan province, China* (736 pp). Beijing: Geological Publishing House (in Chinese with English abstract).  
 Cathelineau, M. (1988). Cation site occupancy in chlorites and illites as a function of temperature. *Clay Minerals*, 23, 471–485.  
 Chen, M., He, W. J., Liang, B., & Xie, Q. X. (2001). Characteristics of very low grade metamorphic rocks in the Xikang Group of northwest Sichuan. *Acta Geologica Sichuan*, 21, 65–69. (in Chinese with English abstract).  
 Chung, S. L., Chu, M. F., Zhang, Y. Q., Xie, Y. W., Lo, C. H., Lee, T. Y., et al. (2005). Tibetan tectonic evolution inferred from spatial

- and temporal variations in post-collisional magmatism. *Earth-Science Reviews*, 68, 173–196.
- Corrado, S., Invernizzi, C., Aldega, L., D'Errico, M., Di Leo, P., Mazzoli, S., et al. (2010). Testing the validity of organic and inorganic thermal indicators in different tectonic settings from continental subduction to collision: The case history of the Calabria-Lucania border (southern Apennines, Italy). *Journal of the Geological Society*, 167, 985–999.
- Cruz, M. D. R., & Jiménez, P. R. (2002). Correlation between crystallochemical parameters of phyllosilicates and mineral facies in very low-grade metasediments of the Betic Cordilleras, Spain: A synthesis. *Clay Minerals*, 37, 169–185.
- Dong, S. D., Shen, Q. H., Sun, D. Z., & Lu, L. Z. (1986). *Metamorphic map of China on a scale of 1/4000000*. Beijing: Geological publishing house.
- Frey, M. (1987). Very low-grade metamorphism of clastic sedimentary rocks. In M. Frey (Ed.), *Low temperature metamorphism* (pp. 9–58). Glasgow and London: Blackie.
- Goldsmith, J. R., Graf, D. R., & Joensun, G. I. (1955). The occurrence of magnesium calcite in nature. *Geochimica et Cosmochimica Acta*, 7, 212–230.
- Goldsmith, J. R., & Newton, R. C. (1969). P-T relations in the system CaCO<sub>3</sub>-MgCO<sub>3</sub> at high temperature and pressures. *American Journal of Science*, 267A, 160–190.
- Guidotti, C. V., & Sassi, F. P. (1986). Classification and correlation of metamorphic facies series by means of muscovite b<sub>0</sub> data from low-grade metapelites. *Neues Jahrbuch für Mineralogie Abhandlungen*, 153, 363–380.
- Guidotti, C. V., & Sassi, F. P. (2002). Constrains on studies of metamorphic K-Na white micas. *Reviews in Mineralogy and Geochemistry*, 46, 413–448.
- Gutiérrez-Alonso, G., & Nieto, F. (1996). White-mica 'crystallinity', finite strain and cleavage development across a large Variscan structure, NW Spain. *Journal of the Geological Society, London*, 153, 287–299.
- Hu, J. M., Meng, Q. R., Shi, Y. R., & Qu, H. J. (2005). SHRIMP U-Pb dating of zircons from granitoid bodies in the Songpan-Garzê terrane and its implications. *Acta Petrologica Sinica*, 21, 867–880. (in Chinese with English abstract).
- Huang, M. H., Buick, I. S., & Hou, L. W. (2003). Tectonometamorphic evolution of the eastern Tibet Plateau: Evidence from the central Songpan-Garze Orogenic Belt, western China. *Journal of Petrology*, 44, 255–278.
- Inoue, A., Meunier, A., Patrier-Mas, P., Rigault, C., Beaufort, D., & Vieillard, P. (2009). Application of chemical geothermometry to low-temperature trioctahedral chlorites. *Clays and Clay Minerals*, 57, 371–382.
- Kemp, S. J., & Merriman, R. J. (2009). Polyphase low-grade metamorphism of the Ingleton Group, northern England, UK: A case study of metamorphic inversion in a mudrock succession. *Geological Magazine*, 146, 237–251.
- Kisch, H. J. (1991). Illite crystallinity: Recommendations on samples preparation, X-ray diffraction settings, and interlaboratory samples. *Journal of Metamorphic Geology*, 9, 665–670.
- Kübler, B. (1964). Les argiles, indicateurs de métamorphisme. *Revue Institut de la Française Pétrole*, 19, 1093–1112.
- Li, Y., Zhou, R. J., Densmore, A. L., Ellis, M. A., & Li, Y. Z. (2006). *Continental dynamics and geological responses of the eastern margin of Qinghai-Tibet plateau* (148 pp.). Beijing: Geological Publishing House (in Chinese with English abstract).
- Ma, Y. S., Cai, X. Y., & Li, G. X. (2005). Basic characteristics and concentration of the Puguang Gas field in the Sichuan Basin. *Acta Geologica Sinica (Chinese edition)*, 79, 858–865.
- Ma, Y. S., Fu, X. Y., Wu, J. S., & Chen, G. (2007). Crustal structural and tectonic evolution and oil prospect evaluation in the Songpan-Zoigê block. *Acta Geologica Sinica (English edition)*, 81, 1–10.
- Ma, L. F., Qiao, X. F., Min, L. R., Fan, B. X., & Ding, X. Z. (2002). *Geological atlas of China* (348 pp.). Beijing: Geological Publishing House (in Chinese).
- Merriman, R. J., & Peacor, D. R. (1999). Very low-grade metapelites: Mineralogy, microfabrics and measuring reaction progress. In M. Frey & D. Robinson (Eds.), *Low grade metamorphism* (pp. 10–60). London: Blackwell.
- Miyashiro, A., & Shido, F. (1985). Tschermak substitution in low- and middle-grade pelitic schists. *Journal of Petrology*, 26, 449–487.
- Mullis, J. (1987). Fluid inclusion studies during very low grade metamorphism. In M. Frey (Ed.), *Low temperature metamorphism* (pp. 162–199). London: Blackwell.
- Mullis, J., Rahn, M. K., Schwer, P., de Capitani, C., Stern, W. B., & Frey, M. (2002). Correlation of fluid inclusion temperatures with illite "crystallinity" data and clay mineral chemistry in sedimentary rocks from the external part of the Central Alps. *Schweizerische Mineralogische und Petrographische Mitteilungen*, 82, 325–340.
- Nie, S. Y., Yin, A., Rowley, D. B., & Jin, Y. G. (1994). Exhumation of the Dabie Shan ultra high-pressure rocks and accumulation of the Songpan-Garzê flysch sequence, central China. *Geology*, 22, 999–1002.
- Offler, R., Phillips, G., Fergusson, C. L., & Green, T. J. (2011). Tectonic implications of early paleozoic metamorphism in the Anakie Inlier, Central Queensland, Australia. *Journal of Geology*, 119, 467–485.
- Padan, A., Kisch, H. J., & Shagam, R. (1982). Use of the lattice parameter b<sub>0</sub> of dioctahedral illite/muscovite for the characterization of P/T gradients of incipient metamorphism. *Contributions to Mineralogy and Petrology*, 79, 85–95.
- Potel, S. (2007). Very low-grade metamorphic study in the pre-Late Cretaceous terranes of New Caledonia (southwest Pacific Ocean). *The Island Arc*, 16, 291–305.
- Pullen, A., Kapp, P., Gehrels, G. E., Vervoort, J. D., & Lin, D. (2008). Triassic continental subduction in central Tibet and Mediterranean-style closure of the Paleo-Tethys Ocean. *Geology*, 36, 351–354.
- Rieder, M., Cavazzini, G., D'Yakonov, Y., Frank-Kamenetskii, V. A., Gottardi, G., Guggenheim, S., et al. (1998). Nomenclature of the micas. *Canadian Mineralogist*, 36, 905–912.
- Roger, F., Jolivet, M., & Malavieille, J. (2008). Tectonic evolution of the Triassic fold belts of Tibet. *Comptes Rendus Geoscience*, 340, 180–189.
- Roger, F., Jolivet, M., & Malavieille, J. (2010). The tectonic evolution of the Songpan-Garzê (North Tibet) and adjacent areas from Proterozoic to Present: A synthesis. *Journal of Asian Earth Sciences*, 39, 254–269.
- Rumble, D. I. I. (1973). Andalusite, kyanite and sillimanite from the Mount Mooselauke Region, New Hampshire. *Geological Society of America Bulletin*, 84, 2423–2430.
- Sassi, F. P., & Scolari, A. (1974). The b<sub>0</sub> value of the potassium white micas as a barometric indicator in low-grade metamorphism of pelitic schists. *Contributions to Mineralogy and Petrology*, 45, 143–152.
- Shannon, R. D. (1976). Revised effective ionic radii and systematic studies of interatomic distances in Halides and Chalcogenides. *Acta Crystallographica*, A32, 751–767.
- She, Z. B., Ma, C. Q., Mason, R., Li, J. W., Wang, G. C., & Lei, Y. H. (2006). Provenance of the Triassic Songpan-Garze flysch, west China. *Chemical Geology*, 231, 159–175.
- Turner, F. J. (1981). *Metamorphic petrology: Mineralogical, field, and tectonic aspects* (524 pp). 2nd edition. New York: McGraw-Hill Book Company, Hemisphere Publishing Corporation.

- Wang, Q. C., & Cai, L. G. (2007). Phanerozoic tectonic evolution of South China. *Acta Geologica Sinica-Chinese Version*, 81, 1025–1040. (in Chinese with English abstract).
- Wang, H., Frey, M., & Stern, W. B. (1996). Diagenesis and metamorphism of clay minerals in the Helvetic Alps of Eastern Switzerland. *Clays and Clay Minerals*, 44, 96–112.
- Wang, H. J., Rahn, M., Tao, X. F., Zheng, N., & Xu, T. J. (2008). Diagenesis and metamorphism of Triassic flysch along profile Zoigê-Lushan, northwest Sichuan, China. *Acta Geologica Sinica*, 82, 917–926.
- Wang, H., Rahn, M., Zhou, J., & Tao, X. (2011). Tectonothermal evolution of the Triassic flysch in the Songpan-Garzê orogen, eastern margin of Tibetan plateau. *Mineralogical Magazine*, 75(3), 2117.
- Warr, L. N., & Rice, A. H. N. (1994). Interlaboratory standardization and calibration of clay mineral crystallinity and crystallite size data. *Journal of Metamorphic Geology*, 12, 141–152.
- Weislogel, A. L. (2008). Tectonostratigraphic and geochronologic constraints on evolution of the northeast Paleotethys from the Songpan-Ganzi complex, central China. *Tectonophysics*, 451, 331–345.
- Weislogel, A. L., Graham, S. A., Chang, E. Z., Wooden, J. L., Gehrels, G. E., & Yang, H. (2006). Detrital zircon provenance of the Late Triassic Songpan-Garzê complex: Sedimentary record of collision of the North and South China blocks. *Geology*, 34, 97–100.
- Xia, Z. S. (1993). Synorogenic regional anchi-metamorphism of Triassic terrigenous clastic rock in Songpan-Garze orogenic belt in early Yanshan epoch. *Acta Geologica Sichuan*, 13, 189–192. (in Chinese with English abstract).
- Xiao, L., Zhang, H. F., Clemens, J. D., Wang, Q. W., Kan, Z. Z., Wang, K. M., et al. (2007). Late Triassic granitoids of the eastern margin of the Tibetan plateau: Geochronology, petrogenesis and implications for tectonic evolution. *Lithos*, 96, 436–452.
- Xu, Z. Q., Hou, L. W., & Wang, Z. X. (1992). *Orogenic processes of the Songpan-Garze orogenic belt of China*. Beijing: Geological publishing house (in Chinese).
- Xu, Z. Q., Yang, J. S., Li, H. B., Zhang, J. X., & Wu, C. L. (2007). *Orogenic plateau-terrane amalgamation, collision and uplift in the Qinghai-Tibet Plateau* (458 pp). Beijing: Geological publishing house (in Chinese with English abstract).
- Yang, C., & Hesse, R. (1991). Clay minerals as indicators of diagenetic and anchimetamorphic grade in an overthrust belt external domain of southern Canadian Appalachians. *Clay Minerals*, 26, 211–231.
- Yang, Q., & Liu, L. W. (2005). Experimental study on diagenetic evolution for Triassic in the Songpan-Aba area. *Petroleum Geology and Experiment*, 27, 534–538. (in Chinese with English abstract).
- You, Z. D., Cheng, S. H., & Lai, X. Y. (2006). The Danba domal metamorphic terrane, western Sichuan, China. *Earth Science Frontiers*, 13, 148–159. (in Chinese with English abstract).
- Zhang, K. J., Li, B., Wei, Q. G., Cai, J. X., & Zhang, Y. X. (2008). Proximal provenance of the western Songpan-Ganzi turbidite complex (Late Triassic, eastern Tibetan plateau): Implications for the tectonic amalgamation of China. *Sedimentary Geology*, 208, 36–44.
- Zhao, D. J., Wu, S., & Wu, D. C. (2004). The stages of the folds and its effect on lithostratigraphy in the Jinping hydropower station region of the Yalong river. *Advance in earth sciences*, 19, suppl., 60–65 (in Chinese with English abstract).
- Zhou, D., & Graham, S. A. (1996). Songpan-Garzê complex of west Qingling Shan as Triassic remnant ocean basin fill trapped during the Mesozoic tectonic amalgamation of China. In A. Yin & M. Harrison (Eds.), *The tectonic evolution of Asia* (pp. 281–299). Cambridge: Cambridge University Press.
- Zhou, M. F., Yan, D. P., Vasconcelos Paulo, M., Li, J. W., & Hu, R. Z. (2008). Structural and geochronological constraints on the tectono-thermal evolution of the Danba domal terrane, eastern margin of the Tibetan plateau. *Journal of Asian Earth Sciences*, 33, 414–427.